

Efficient loading of thulium atoms in a compact MOT for a transportable optical clock

A. Golovizin,* D. Tregubov, D. Mishin, and D. Provorchenko

P.N. Lebedev Physical Institute, Leninsky prospekt 53, 119991 Moscow, Russia

N. Kolachevsky

P.N. Lebedev Physical Institute, Leninsky prospekt 53, 119991 Moscow, Russia and

Russian Quantum Center, Bolshoy Bulvar 30,

bld. 1, Skolkovo IC, 121205 Moscow, Russia

(Dated: May 6, 2021)

Abstract

We report on building of a compact vacuum chamber for spectroscopy of ultracold thulium and trapping of up to 13 million atoms. Compactness is achieved by obviating a classical Zeeman slower section and placing an atomic oven close to a magneto-optical trap (MOT), specifically at the distance of 11 cm. In this configuration, we significantly gained in solid angle of an atomic beam, which is affected by MOT laser beams, and reached 1 million atoms loaded directly in the MOT. By exploiting Zeeman-like deceleration of atoms with an additional laser beam, we increased the number of trapped atoms to 6 million. Then we gained an extra factor of 2 by tailoring the MOT magnetic field gradient with an additional small magnetic coil. Demonstrated results show great perspective of the developed setup for realizing a compact high-performance optical atomic clock based on thulium atoms.

*Electronic address: artem.golovizin@gmail.com

I. INTRODUCTION

Rapid progress in the field of high-precision optical atomic clocks translated into numerous applications like relativistic geodesy and gravimetry [1, 2], global timekeeping and synchronization [3, 4], navigation [5] as well as delicate tests of fundamental physics [6–9]. To satisfy the growing demands [10], transportable systems with relative systematic uncertainty and instability at the 10^{-17} level or better are required. Besides technical difficulties, one of the main challenges is to establish tight control over the environmental influence on the clock transition frequency. The leading perturbation factors are the external magnetic and electric fields [11, 12] (including blackbody radiation (BBR)), which can shift the frequency at the 10^{-14} level and require a special approach to compensate for.

Single-ion-based optical clocks are typically more robust compared to atomic clocks based on neutral atoms because of the deep trapping potential, long ion life time and small BBR shift for the ion systems. The ultimate relative instability and inaccuracy for both clock types is now approaching the 10^{-18} level [13–15], however, single-ion clocks require much longer averaging time due to lower statistics. Indeed, neutral-atom clocks typically operate with ensembles of 10^3 - 10^4 neutral atoms in an optical lattice, compared to a single ion in a Paul trap. For many applications like geodesy and navigation, averaging time plays a crucial role which points towards neutral atoms being a favorable platform. On the other hand, neutral atom clocks typically possess higher sensitivity to external electromagnetic (EM) fields compared to ion clocks. Another challenge is to design a compact and robust vacuum system. An intensive flux of initially hot atoms should be decelerated and loaded into a magneto-optical trap (MOT), which is commonly done with the help of a Zeeman slower [16]. Moreover, a delicate optical cavity forming an optical lattice should be incorporated into the vacuum system. The transportable Sr optical clocks [2, 17] possess a few- m^3 -size which is still significantly more compared to the demonstrated ion-based systems [18, 19]. To achieve the ultimate clock performance, cryogenic vacuum techniques are used to provide suppression of the BBR shift [2, 20]. Therefore, it would be desirable to combine the advantages of ion-based clocks (small size, robustness and low sensitivity to EM fields) with those of neutral atom clocks (good statistics, low short-time frequency instability).

We have experimentally demonstrated a number of attractive features of the inner-shell magnetic-dipole transition in neutral thulium at $1.14\ \mu\text{m}$ [21, 22]. Its frequency possesses

very low sensitivity to BBR, namely 3000 times lower compared to the Sr metrological transition at 698 nm. The magic wavelength is close to 1064 nm where powerful low-phase-noise lasers are available. Moreover, the bicolor operation [23, 24] based on simultaneous interrogation of two hyperfine transitions allows us to cancel out the quadratic Zeeman shift. Our analysis [25] shows that Tm optical lattice clocks at room temperature can reach the low 10^{-18} level of total systematic frequency shift. This drastically softens requirements for the external parameters like thermal surroundings, magnetic field stability, as well as the spectral purity and frequency stability of the optical lattice laser. All these features are highly desirable for development of a transportable optical clock operating below the 10^{-17} level of fractional instability and inaccuracy. In this paper, we focus on development of a compact and robust thulium MOT assembly which is the key part of a clock system.

For alkali atoms with high vapor pressure (like Rb), compact MOTs with high loading rates have been known for decades, and great progress in their miniaturization was achieved recently with the pyramid [26, 27] and grating [28, 29] configurations. However, most of the atomic species used today for the high-performance optical clocks have low vapor pressure at room temperature, so high-temperature ovens are necessary. The oven is typically placed far apart from the MOT region for two reasons. First, a Zeeman slower of a certain length (a few tens of cm) is typically required to decelerate atoms from the thermal speed to the MOT's capture velocity. Second, thermal radiation from the hot oven induces an additional BBR shift of the clock transition frequency (proportional to T^4 , T is the temperature). Proximity of the oven also induces undesirable collisions.

In recent years, significant progress has been made on the route of compactization of the optical clock setups. To begin with, Zeeman-free systems with a 2D-MOT for initial slowing of atoms [30, 31] were demonstrated. These configurations significantly reduce the system size and lift up some undesirable effects (like hot atomic beam, direct view of the oven, power consumption of Zeeman coils or magnetic field from permanent magnets), but they still require an extra volume for pre-cooling and increase complexity of the system. Beside this, the pyramid [32] and grating [33] MOTs for Sr atoms were developed. An interesting approach with laser ablation of atoms was implemented in refs. [34, 35].

In this work, we demonstrate experimental realization of a compact thulium MOT without the use of the “classical” Zeeman slower section. The MOT is efficiently loaded directly from the atomic oven placed in the proximity of the MOT region. Very low sensitivity of

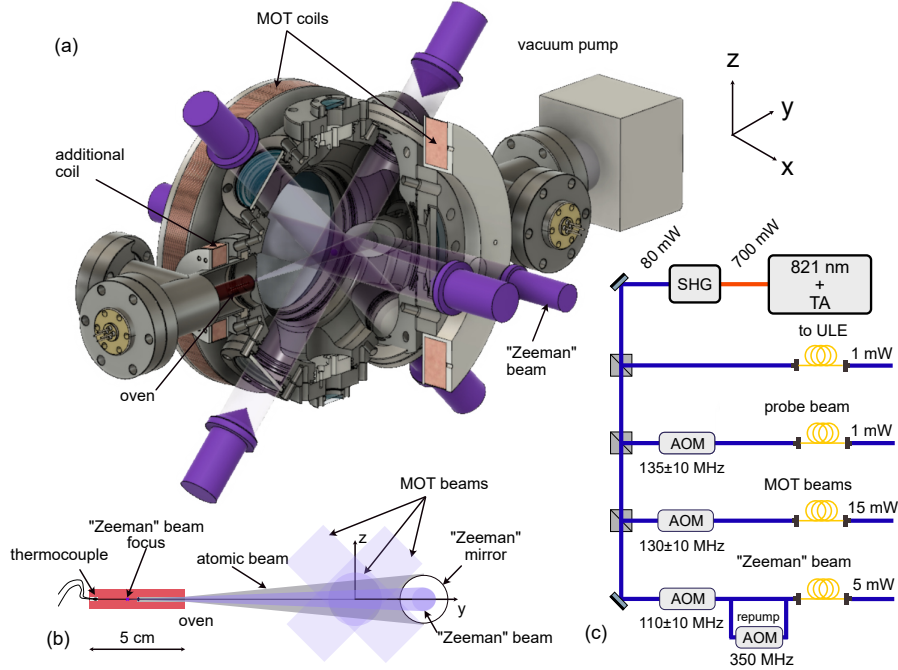


Figure 1: The experimental setup. (a) The 3D model of the experimental vacuum chamber. The cooling (MOT) and decelerating (“Zeeman”) laser beams are shown with purple arrows. (b) The sketch of the atomic oven and the cooling beams. (c) The optical scheme. The output of the second harmonic generation (SHG) cavity at 410.7 nm is split in four beams. The MOT, “Zeeman” and probe laser beams are frequency shifted by the acousto-optic modulators (AOMs) and delivered to the vacuum chamber with the optical fibers (yellow curves). The repumper radiation $|g, F = 3\rangle \rightarrow |b, F = 4\rangle$ is added to the “Zeeman” beam.

the $1.14 \mu\text{m}$ clock transition frequency to BBR ensures small impact of the oven radiation. We simulated the atom capture process in our setup in order to optimize the magnetic field configuration and to evaluate the MOT’s loading rate. Two different configurations with 6 or 7 laser beams (one additional beam for deceleration) were analyzed, both offering prospects of the loading rate of more than 10^6 atoms/s.

The manuscript is organized as follows: the Section II describes the vacuum chamber geometry and laser cooling beams configuration. The Section III is devoted to a brief description of our numerical model. In the Section IV, we demonstrate experimental results. Finally, we sum up the conclusions in the Section V.

II. SETUP

The main part of the the experimental apparatus is shown in Fig.1.a. We use a 6-inch spherical octagon vacuum chamber from Kimball Physics Inc. [36] . The atomic oven is mounted inside the CF40 T-flange. The non-evaporable getter pump Z100 from SAES Group [37], the angle valve and the electrical feedthrough for the in-vacuum-mounted optical lattice enhancement cavity are connected to the main chamber with the CF40 cross. One of the 3 orthogonal pairs of the MOT beams goes through the center of CF100 windows along the x axis, while the other two orthogonal beam pairs lay in the $z - y$ plane and pass through CF40 windows. This configuration is further referred to as the 6-beam MOT. In the 7-beam MOT, we use an additional, focused “Zeeman” laser beam which is parallel to the x axis. It is deflected by an in-vacuum elliptical-shape mirror opposite to the atomic beam emitted by the oven. This allows us to achieve good “Zeeman” beam convergence on the oven and prevent optical windows from metal deposition. The probe laser beam goes in the horizontal plane and is not shown. Coils for the MOT’s magnetic quadrupole field are mounted on the CF100 flanges, each coil containing 546 loops of a 1-mm diameter copper wire. The magnetic field gradient at the MOT center equals 14 G/cm (along the x axis) per 1 A current. An additional pair of magnetic coils is installed axially to the y direction which allows one to modify the magnetic field profile along the atomic beam, which is discussed in the Sec. IV B.

A more detailed sketch of the atomic oven is shown in Fig. 1.b. The oven is made from a 50 mm-long, 10 mm-diameter ruby rod. Metallic thulium is loaded into a $L = 25$ mm-deep hole with a diameter of $d = 2.5$ mm. The atomic beam divergence is approximately $\Delta\theta = d/L = 0.1$ rad. The oven surface is homogeneously heated by a 0.2 mm-diameter tungsten wire. A thermocouple is attached to the ruby rod to measure the oven temperature. To achieve an atomic flux of $\Phi \approx 10^{10}$ atoms/s at the oven’s exit, one needs to heat the oven to 500 °C, which requires 20 W of electrical power.

The optical part of the setup is shown in Fig. 1.c. For laser cooling of thulium atoms we use a strong cooling transition $|g, F = 4\rangle \rightarrow |b, F = 5\rangle$ at 410.7 nm with a natural linewidth of $\gamma = 10$ MHz [38]. Here, $|g\rangle$ denotes the ground level and $|b\rangle$ — the upper cooling level, F is the total momentum of the atom. A 821 nm semiconductor laser with a tapered amplifier (Sacher Lasertechnik Group [39]) and a home-made second harmonic generation cavity [40]

provides 80 mW of 410.7 nm radiation. The laser frequency is stabilized to a ULE cavity mode. The probe, “Zeeman”, repumping and MOT cooling beams are frequency shifted and modulated by corresponding acousto-optic modulators (AOMs). Optical radiation is delivered to the vacuum apparatus by 3 optical fibers. In this configuration, we get 15 mW radiation at 410.7 nm for the MOT beams and 1 mW for the resonant probe beam. The MOT beams radii ($1/e^2$ intensity level) equal $w_{\text{MOT}} = 14$ mm. The input beams apertures are limited by 30 mm collimation lenses, while the back-reflected beams are truncated by 22 mm-diameter quarter-waveplates. The probe beam has a radius of 1.15 mm. Frequency of the probe beam was set close to the exact transition resonance.

III. MOT LOADING SIMULATIONS

We performed Monte-Carlo trajectory simulation of atoms defused from the atomic oven interacting with the cooling laser beams. Our approach is similar to the one described in Ref. [30]. For every set of parameters, we calculated $n_{\text{tot}} = 1000$ atomic trajectories using the 4th-order Runge-Kutta algorithm with a time step of $\delta t = 50 \mu\text{s}$. We assumed that an atom was trapped if its final coordinate was closer than $0.5 w_{\text{MOT}}$ from the MOT center, where w_{MOT} is the MOT cooling beams radii.

A. Initial parameters

The initial position of atoms was fixed at the oven center $\mathbf{r}_0 = (0, y_{\text{oven}}, 0)$. Here, $y_{\text{oven}} = -11.4$ cm is the distance from the MOT center to the oven (see Fig. 1.b). The initial velocity vector was chosen randomly from the uniform distribution within a cone with an opening angle of $2\Delta\theta$. The velocity modulus was sampled from the Maxwell-Boltzman distribution for the oven temperature $T = 500^\circ\text{C}$ truncated at v_{th} . The velocity threshold v_{th} was estimated by analyzing the capture process of atoms moving along the y axis, i.e. with the initial velocity $\mathbf{v} = (0, v, 0)$. For different MOT parameters, v_{th} lay between 35 and 150 m/s. The capture efficiency was inferred as $\zeta = n_{\text{trapped}}/n_{\text{tot}} \times \eta(v_{\text{th}})$, where $\eta(v_{\text{th}})$ is the fraction of atoms in the truncated part of the Maxwell-Boltzman distribution.

The total atomic flux was evaluated using an expression for a capillary output:

$$\Phi = \frac{4\sqrt{\pi}}{3} \frac{n_{\text{ov}} v_{\text{th}} d^3}{8L}, \quad (1)$$

where n_{ov} is the thulium atomic vapor density [41] and v_{th} is the most probable thermal velocity at $T = 500^\circ\text{C}$. This assumption may differ from our experimental situation because the expression (1) corresponds to the case when the capillary of length L and diameter d is connected to a reservoir of atomic vapor at a certain temperature. In our case, a chunk of sublimating metal is placed in the capillary.

B. Atom-light interaction

Atom-light interaction was considered as a classical friction-type force induced by the photon scattering on a 2-level-system:

$$\mathbf{F} = \hbar k \sum_i R_i^{\text{sc}} \hat{\mathbf{k}}_i + \hbar k \sqrt{N^{\text{sc}}} \mathbf{e}_r \quad (2)$$

Here, \hbar is the reduced Plank constant, $k = 2\pi/\lambda_{410}$. Summation goes over all optical beams (see Fig. 1) with the unit wave vectors $\hat{\mathbf{k}}_i = \mathbf{k}_i/k$ and the i th beam scattering rate of R_i^{sc} . The last term is responsible for heating from spontaneous emission. It introduces a momentum kick in a random direction \mathbf{e}_r proportional to $N^{\text{sc}} = \delta t \sum_i R_i^{\text{sc}}$.

For every time stamp we calculated i th beam scattering rate

$$R_i^{\text{sc}} = \frac{\Gamma}{2} \frac{s_i}{1 + s_i + 4(\Delta_i/\Gamma)^2} \quad (3)$$

based on the atom's coordinate \mathbf{r} and velocity \mathbf{v} from the previous step. Here, $s_i = s_i^0 \exp\left(-\frac{2|\mathbf{r} \times \hat{\mathbf{k}}_i|^2}{w_i^2}\right)$ is the saturation parameter for the i th beam with a waist of w_i and on-axis saturation parameter of s_i^0 . For the MOT beams, w_i and s_i^0 are constant, while for the ‘‘Zeeman’’ beam they depend on the y coordinate. In order to take into account finite beams apertures, we set s_i to zero when $|\mathbf{r} \times \hat{\mathbf{k}}_i| \geq r_{\text{lens}}$. Effective detuning of the i th beam from the exact resonance is calculated as $\Delta_i = \Delta_i^0 + (\mathbf{k}_i, \mathbf{v}) - g_b \mu_B / \hbar B(\mathbf{r}) \sigma_i$. Here, Δ_i^0 is the frequency detuning of the i th beam (either $2\pi\Delta\nu_{\text{MOT}}$ or $2\pi\Delta\nu_Z$), $g_b = 1$ is the Lande g-factor of the upper cooling level, $B(\mathbf{r})$ is the magnetic field and $\sigma_i = \pm 1$ is the coefficient related to the beam polarization. One can not consider cooling beams independently when $R^{\text{sc}} = \sum_i R_i^{\text{sc}}$ is larger than $\Gamma/2$ (the maximum photon scattering rate on the transition). To avoid this, we used normalized scattering rates $\tilde{R}_i^{\text{sc}} = R_i^{\text{sc}} / (1 + 2(R^{\text{sc}} - R_i^{\text{sc}})/\Gamma)$ in Eq. 2.

IV. RESULTS

A. 6-beam MOT

Simulations predicted that about 10^{-5} fraction of total atomic flux from the oven could be trapped in the 6-beam MOT. This corresponds to the loading rate of $10^5 - 10^6$ atoms/s. The pulse sequence of the experiment is the following: the MOT is loaded during $t_{\text{load}} = 0.2 - 4$ s with the MOT laser beams and quadrupole magnetic field on. We switch off the MOT laser beams (using AOM) and magnetic field, and after 1 ms interval the number of atoms is measured using fluorescence signal from the resonant 410 nm beam recorded by a CMOS camera. Then we wait for $t_{\text{wait}} = 0.5 - 1$ s before the next loading cycle.

We measure the number of atoms in the 6-beams MOT after $t_{\text{load}} = 3$ s loading time as a function of the cooling beams frequency detuning and value of the quadrupole magnetic field, as it is shown in Fig. 2.a. The frequency is scanned using a single-pass AOM. To compensate for variations of the diffraction efficiency and optical fiber coupling, we apply feed-forward on the AOM's RF drive power according to the calibration. In this configuration we trap up to 10^6 Tm atoms.

B. 7-beam MOT

Regarding the number of atoms, the 6-beam MOT can already be used for optical clock applications. However, our simulations show that the MOT magnetic field gradient can be used for a Zeeman-like slowing of the atoms escaping the oven with an additional “Zeeman” laser beam (see Fig. 1.b) directed opposite to the atomic flux. We use the “Zeeman” beam with a convergence of $\Theta = 0.1$ rad (2 times smaller than the atomic beam divergence, currently limited by the out-of-vacuum optics). The beam radius at the MOT center equals $w_z = 5$ mm. The implemented configuration allows one to:

1. reduce blowing-out of atoms from the MOT by the “Zeeman” beam.
2. decelerate atoms opposite to their velocities instead of along the y axis (the “Zeeman” beam direction).

The pulse sequence is the same as for the 6-beam MOT. After certain optimization, we measure the number of trapped atoms in the 7-beam MOT for different magnetic field

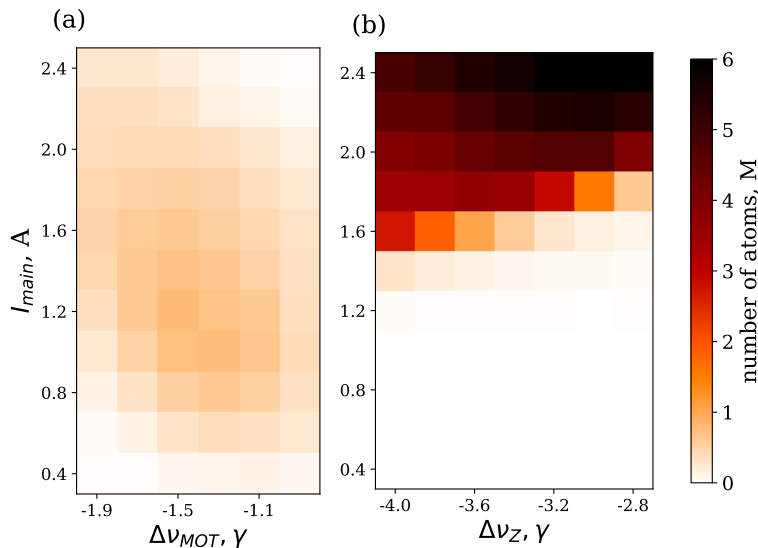


Figure 2: (a) Experimentally measured number of atoms in the 6-beam MOT as a function of the current flowing through the MOT magnetic coils (proportional to the field gradient) and the frequency detuning of the MOT cooling beams $\Delta\nu_{\text{MOT}}$. (b) Similar plot for the 7-beam MOT, but in this case we scan the frequency detuning of the Zeeman beam $\Delta\nu_{\text{Z}}$. The color bar is common for both plots.

gradients and “Zeeman” beam detunings as shown in Fig. 2.b. We observe a relatively sharp edge which separates the region with efficient trapping from the region where almost no atoms are captured. This corresponds to the resonance condition for the “Zeeman” laser beam at a certain magnetic field gradient. In this configuration we reached 6 millions atoms in the MOT.

We also study dependency of the trapping efficiency on the fraction of optical power in the “Zeeman” beam $\eta_{P_{\text{Z}}} = P_{\text{Z}}/(P_{\text{Z}} + P_{\text{MOT}})$ (Fig. 3.a). Starting from $\eta_{P_{\text{Z}}} = 0.35$, it rapidly decreases since the “Zeeman” beam pushes equilibrium cloud position outside intersection of the MOT beams. Simulations shown in the same figure confirm the observed behavior within the simulation uncertainty (the shaded area). The number of trapped atoms in all simulations are scaled by a factor of $\xi = 0.8$ to achieve the best matching with the experimental data shown in Fig. 3.a.

One can see from Fig. 2.b that the increase of current I_{main} in the 7-beam MOT results in the continuous growth of the number of atoms (which is also confirmed by simulations).

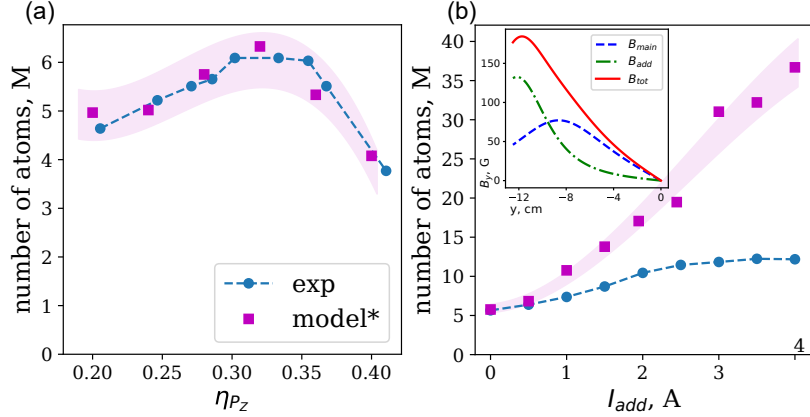


Figure 3: (a) The maximum number of atoms in the 7-beam MOT as a function of fraction of optical power in the “Zeeman” beam ηP_z . (b) The number of atoms as a function of current I_{add} through the additional coil pair at $I_{main} = 2.4$ A. The experimental data is shown in blue circles, the simulation is shown in red squares, the estimated uncertainty (statistical) of the simulation is depicted with the shaded area. Inset in (b) shows the magnetic field profile along the y axis produced by the main coils at $I_{main} = 2.4$ A (blue dashed line), additional coils at $I_{add} = 4$ A (green dashed-dotted line), and their sum (red solid line).

In our case, it was limited by technical reasons since $I_{main} = 2.4$ A corresponds to about 100 W power dissipation which is already at the edge of the practical use. As an alternative approach to increase I_{main} further, we used the additional coil pair (see Fig. 1.a). These coils modify the magnetic field profile along the y axis making its gradient more uniform as it is shown in the inset of Fig.3.b. According to our simulations, this should raise by 20 – 40 m/s the maximum trapping velocity of atoms and significantly increase the loading rate.

Working in the optimal configuration (determined from the Fig. 2.b), we observe a two times increase of the number of atoms in MOT when changing the additional coils current I_{add} from 0 to 4 A, as shown in Fig.3.b. It is much less than expected from the model (red dots and the shaded area). The discrepancy is most probably due to the Zeeman structure of thulium energy levels. This issue is considered in more details in the Supplementary Material.

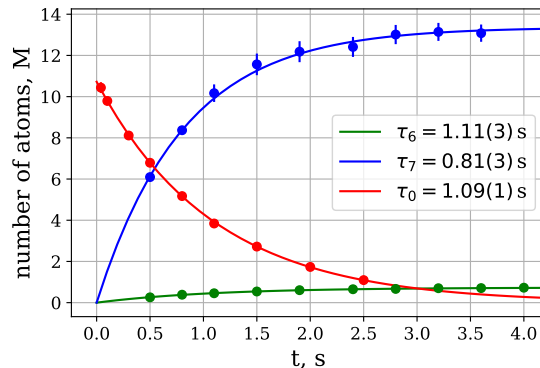


Figure 4: The loading and the loss dynamics of the 6-beam (green) and the 7-beam (blue and red) MOTs. The legend shows time constants inferred from the fits (see text). Number of atoms is in millions.

C. Loading dynamics

The loading dynamics at the optimal parameters for the 6-beam and 7-beam MOTs are presented in Fig. 4 with green and blue dots, correspondingly. The experimental data are fitted by the exponential function $N_{\text{load}}(t) = R \times \tau(1 - e^{-t/\tau})$ giving the time constant $\tau_6 = 1.11(4)$ s and loading rate $R_6 = 0.66(2) \times 10^6$ atoms/s for the 6-beam MOT, and $\tau_7 = 0.81(4)$ s and $R_7 = 16.5(5) \times 10^6$ atoms/s for the 7-beam MOT. The lifetime of atoms in the MOT is measured by switching off the 7-beam MOT loading (turning off the “Zeeman” beam) and measuring the number of atoms as a function of holding time (red dots). The experimental data is fitted by the exponential decay function $N_{\text{loss}}(t) = N_0 e^{-t/\tau_0}$ (red solid line). The MOT lifetime equals $\tau_0 = 1.09(1)$ s, which agrees well with the loading time constant τ_6 . The observed atoms lifetime in the MOT also indicates proper vacuum conditions sufficient for interrogation of the clock transition in the optical lattice.

V. CONCLUSION

On the way to transportable optical clock operating on the inner-shell transition at $1.14 \mu\text{m}$ in Tm, we designed and built the compact MOT system without a traditional Zeeman slower section and demonstrated trapping of up to 13 millions atoms. In this setup, we can load about 1 million atoms just in 100 ms which can considerably increase duty cycle

of the compact clock setup. The observed lifetime of atoms in the MOT exceeds 1 second which points to proper vacuum conditions and low collision rate with atoms from the oven. To prevent an envisioned impact of thermal radiation and atomic flux from the hot oven on the clock transition frequency, we install a mechanical shutter between the oven and the MOT. With all lasers being available from our “stationary” system, we expect rapid implementation of further steps needed to run the optical clock in the developed setup: deep second-stage laser cooling, trapping of atoms into the optical lattice and clock transition spectroscopy.

We believe that the number of trapped atoms can be significantly increased, if necessary (e.g. for experiments with Bose-Einstein condensates [42]), with the further straightforward steps: raising the oven temperature, increasing the optical power per each laser beam and the convergence angle of the “Zeeman” beam. The ongoing development of deep laser cooling of thulium down to $1\ \mu\text{K}$ [43] may open new applications for cold thulium atoms, e.g. as a platform for atomic interferometry and gravimetry.

VI. ACKNOWLEDGEMENTS

The authors acknowledge the support of RSF Grant No. 19-72-00174. We are grateful to Vadim Sorokin for invaluable help with building the thulium oven.

-
- [1] J. Grotti, S. Koller, S. Vogt, S. Häfner, U. Sterr, C. Lisdat, H. Denker, C. Voigt, L. Timmen, A. Rolland, et al., *Nature Physics* **14**, 437 (2018), ISSN 17452481, URL <http://dx.doi.org/10.1038/s41567-017-0042-3>.
 - [2] M. Takamoto, I. Ushijima, N. Ohmae, T. Yahagi, K. Kokado, H. Shinkai, and H. Katori, *Nature Photonics* **14**, 411 (2020), ISSN 17494893, URL <http://dx.doi.org/10.1038/s41566-020-0619-8>.
 - [3] F. Riehle, *Nature Photonics* **11**, 25 (2017), ISSN 1749-4885, URL <http://www.nature.com/doifinder/10.1038/nphoton.2016.235>.
 - [4] J. Yao, J. A. Sherman, T. Fortier, H. Leopardi, T. Parker, W. McGrew, X. Zhang, D. Nicolodi, R. Fasano, S. Schäffer, et al., *Physical Review Applied* **12**, 044069 (2019) (2019), ISSN 2331-

- 7019, URL <https://doi.org/10.1103/PhysRevApplied.12.044069>.
- [5] G. Giorgi, T. D. Schmidt, C. Trainotti, R. Mata-Calvo, C. Fuchs, M. M. Hoque, J. Berdermann, J. Furthner, C. Günther, T. Schuldt, et al., *Advances in Space Research* **64**, 1256 (2019), ISSN 18791948.
- [6] C. J. Kennedy, E. Oelker, J. M. Robinson, T. Bothwell, D. Kedar, W. R. Milner, G. E. Marti, A. Derevianko, and J. Ye, *Physical Review Letters* **125**, 201302 (2020), ISSN 0031-9007, URL <https://link.aps.org/doi/10.1103/PhysRevLett.125.201302>.
- [7] C. Sanner, N. Huntemann, R. Lange, C. Tamm, E. Peik, M. S. Safronova, and S. G. Porsev, *Nature* **567**, 204 (2019), ISSN 0028-0836, URL <http://arxiv.org/abs/1809.10742><http://www.nature.com/articles/s41586-019-0972-2>.
- [8] P. Wcisło, P. Ablewski, K. Beloy, S. Bilicki, M. Bober, R. Brown, R. Fasano, R. Ciuryło, H. Hachisu, T. Ido, et al., *Science Advances* **4**, 1 (2018), ISSN 2375-2548, URL <https://advances.sciencemag.org/lookup/doi/10.1126/sciadv.aau4869>.
- [9] K. Beloy, M. I. Bodine, T. Bothwell, S. M. Brewer, S. L. Bromley, J.-S. Chen, J.-D. Deschênes, S. A. Diddams, R. J. Fasano, T. M. Fortier, et al., *Nature* **591**, 564 (2021), ISSN 0028-0836, URL <http://www.nature.com/articles/s41586-021-03253-4>.
- [10] F. Riehle, P. Gill, F. Arias, and L. Robertsson, *Metrologia* **55**, 188 (2018), ISSN 16817575.
- [11] N. Poli, C. Oates, P. Gill, and G. Tino, *La rivista del Nuovo Cimento* **36** (2013), ISSN 0034-6861, URL <https://link.aps.org/doi/10.1103/RevModPhys.87.637>.
- [12] A. Ludlow, M. Boyd, J. Ye, E. Peik, and P. Schmidt, *Reviews of Modern Physics* **87**, 637 (2015), ISSN 0393697X, URL <http://arxiv.org/abs/1407.3493>.
- [13] N. Huntemann, C. Sanner, B. Lipphardt, C. Tamm, and E. Peik, *Physical Review Letters* **116**, 063001 (2016), ISSN 0031-9007, URL <http://link.aps.org/doi/10.1103/PhysRevLett.116.063001>.
- [14] T. L. Nicholson, S. L. Campbell, R. B. Hutson, G. E. Marti, B. J. Bloom, R. L. McNally, W. Zhang, M. D. Barrett, M. S. Safronova, G. F. Strouse, et al., *Nature Communications* **6** (2015), ISSN 20411723.
- [15] W. F. McGrew, X. Zhang, R. J. Fasano, S. A. Schäffer, K. Beloy, D. Nicolodi, R. C. Brown, N. Hinkley, G. Milani, M. Schioppo, et al., *Nature* **564**, 87 (2018), ISSN 14764687, URL <http://dx.doi.org/10.1038/s41586-018-0738-2>.
- [16] W. D. Phillips and H. Metcalf, *Phys. Rev. Lett.* **48**, 596 (1982), URL <https://link.aps.org/doi/10.1103/PhysRevLett.48.596>.

- [org/doi/10.1103/PhysRevLett.48.596](https://doi.org/10.1103/PhysRevLett.48.596).
- [17] S. Koller, J. Grotti, A. Al-Masoudi, S. Vogt, S. Dorscher, S. Hafner, U. Sterr, and C. Lisdat, *Physical Review Letters* **116**, 063001 (2017), ISSN 0031-9007, URL <http://link.aps.org/doi/10.1103/PhysRevLett.116.063001>.
- [18] J. Cao, P. Zhang, J. Shang, K. Cui, J. Yuan, S. Chao, S. Wang, H. Shu, and X. Huang, *Applied Physics B* **123**, 112 (2017), ISSN 0946-2171, URL <http://arxiv.org/abs/1607.03731><http://dx.doi.org/10.1007/s00340-017-6671-5><http://link.springer.com/10.1007/s00340-017-6671-5>.
- [19] I. V. Zalivako, I. A. Semerikov, A. S. Borisenko, M. D. Aksenov, P. A. Vishnyakov, P. L. Sidorov, N. V. Semenina, A. A. Golovizin, K. Y. Khabarova, and N. N. Kolachevsky, *Quantum Electronics* **50**, 850 (2020), ISSN 1063-7818.
- [20] I. Ushijima, M. Takamoto, M. Das, T. Ohkubo, and H. Katori, *Nature Photonics* **9**, 1 (2015), ISSN 1749-4885, URL <http://www.nature.com/doi/10.1038/nphoton.2015.5>.
- [21] D. Sukachev, S. Fedorov, I. Tolstikhina, D. Tregubov, E. Kalganova, G. Vishnyakova, A. Golovizin, N. Kolachevsky, K. Khabarova, and V. Sorokin, *Phys. Rev. A* **94**, 022512 (2016).
- [22] A. Golovizin, E. Fedorova, D. Tregubov, D. Sukachev, K. Khabarova, V. Sorokin, and N. Kolachevsky, *Nature Communications* **10**, 1 (2019), ISSN 2041-1723, URL <http://dx.doi.org/10.1038/s41467-019-09706-9>.
- [23] E. Fedorova, A. Golovizin, D. Tregubov, D. Mishin, D. Provorchenko, V. Sorokin, K. Khabarova, and N. Kolachevsky, *Physical Review A* **102**, 63114 (2020).
- [24] A. Golovizin, D. Tregubov, E. Fedorova, D. Mishin, D. Provorchenko, K. Khabarova, V. Sorokin, and N. Kolachevsky, in preparation (2021).
- [25] A. Golovizin, D. Tregubov, E. Fedorova, D. Mishin, D. Provorchenko, D. Sukachev, K. Khabarova, V. Sorokin, and N. Kolachevsky, **2241**, 20016 (2020), URL <https://doi.org/10.1063/5.0011462>.
- [26] J. Arlt, O. Marago, S. Webster, S. Hopkins, and C. Foot, *Optics communications* **157**, 303 (1998).
- [27] Q. Bodart, S. Merlet, N. Malossi, F. P. Dos Santos, P. Bouyer, and A. Landragin, *Applied Physics Letters* **96**, 134101 (2010).
- [28] C. Nshii, M. Vangeleyn, J. P. Cotter, P. F. Griffin, E. Hinds, C. N. Ironside, P. See, A. Sinclair,

- E. Riis, and A. S. Arnold, *Nature nanotechnology* **8**, 321 (2013).
- [29] D. Barker, E. Norrgard, N. Klimov, J. Fedchak, J. Scherschligt, and S. Eckel, *Physical review applied* **11**, 064023 (2019).
- [30] M. Barbiero, M. G. Tarallo, D. Calonico, F. Levi, G. Lamporesi, and G. Ferrari, *PHYSICAL REVIEW APPLIED* **13**, 14013 (2020).
- [31] I. Nosske, L. Couturier, F. Hu, C. Tan, C. Qiao, J. Blume, Y. H. Jiang, P. Chen, and M. Weidemüller, *Physical Review A* **96**, 053415 (2017), ISSN 2469-9926, URL <https://link.aps.org/doi/10.1103/PhysRevA.96.053415>.
- [32] W. Bowden, R. Hobson, I. R. Hill, A. Vianello, A. Silva, H. S. Margolis, P. E. G. Baird, P. Gill, M. Schioppo, A. Silva, et al., *Scientific Reports* **9**, 1 (2019), ISSN 20452322, URL <https://doi.org/10.1038/s41598-019-48168-3>.
- [33] A. Sitaram, P. K. Elgee, G. K. Campbell, N. N. Klimov, S. Eckel, and D. S. Barker, *Review of Scientific Instruments* **91**, 103202 (2020), ISSN 10897623, URL <http://aip.scitation.org/doi/10.1063/5.0019551>.
- [34] M. Yasuda, T. Tanabe, T. Kobayashi, D. Akamatsu, T. Sato, and A. Hatakeyama, *Journal of the Physical Society of Japan* **86**, 18 (2017), ISSN 13474073.
- [35] O. Kock, W. He, D. Świerad, L. Smith, J. Hughes, K. Bongs, and Y. Singh, *Scientific Reports* **6**, 37321 (2016), ISSN 2045-2322, URL <http://www.nature.com/articles/srep37321>.
- [36] <https://www.kimballphysics.com/shop/multi-cf-hardware/mcf600-sphoct-f2c8>.
- [37] <https://www.saesgetters.com/products/nextorr-pumps>.
- [38] D. Sukachev, A. Sokolov, K. Chebakov, A. Akimov, S. Kanorsky, N. Kolachevsky, and V. Sorokin, *Physical Review A* **82**, 011405 (2010), ISSN 10502947.
- [39] <https://www.sacher-laser.com>.
- [40] T. Shpakovsky, I. Zalivako, I. Semerikov, A. Golovizin, A. Borisenko, K. Y. Khabarova, V. Sorokin, and N. Kolachevsky, *Journal of Russian Laser Research* **37**, 440 (2016).
- [41] D. Sukachev, Ph.D. thesis, P.N. Lebedev Physical Institute of RAS, Moscow, Russia (2013).
- [42] E. T. Davletov, V. V. Tsyganok, V. A. Khlebnikov, D. A. Pershin, D. V. Shaykin, and A. V. Akimov, *Physical Review A* **102**, 011302 (2020), ISSN 2469-9926, URL <https://link.aps.org/doi/10.1103/PhysRevA.102.011302>.
- [43] D. Provorchenko, D. Tregubov, D. Mishin, A. Golovizin, E. Fedorova, K. Khabarova, V. Sorokin, and N. Kolachevsky, *Quantum Electronics* **5** (2021).

Supplemental Material

From our simulations we optimized the trap configuration, namely, the beams directions, radii and the expected frequency detunings, as well as the magnetic field gradient. It allowed us to properly design the vacuum chamber and the optical setup. Numerical simulations gave us valuable hints on the ways to increase the number of trapped atoms such as implementation of the converging “Zeeman” beam and additional magnetic coils to optimize the magnetic field gradient. Taking into account simplifications used in the modeling, we expect only modest agreement between the theory and experiment.

The model does not take into account the following aspects:

- S1. the Zeeman structure of the ground and the upper cooling levels;
- S2. deviation of the laser beam polarization from σ^+ outside the beam axis, where the magnetic field direction is not collinear with the beam wave vector;
- S3. the decay channels from the upper level to the intermediate levels;
- S4. off-resonant excitation of the $|b, F = 4\rangle$ state and subsequent decay to the $|g, F = 3\rangle$ level;
- S5. deviation of the atomic flux from the capillary velocity distribution.

Note, that the simulations reasonably well reproduce the experimentally observed number of trapped atoms as a function of the parameter η_{P_z} (Fig. 3.a). One also observes good agreement for the “Zeeman” beam detuning and magnetic field gradient dependencies (Fig. 2.b and Fig. 5.c) (7-beam MOT configuration). In these cases the atom-light interaction seems to be close to that of the 2-level system and the effects which are discussed below do not play a significant role.

Noticeable disagreement between simulation and experiment are observed in the following cases:

1. The capture efficiency *vs.* I_{add} (Fig. 3.b). It is probably associated with neglecting the Zeeman levels structure in the model. The frequencies of σ^+ (as well as σ^- and π) transitions from different m_F states are almost equal in the presence of the magnetic field owing to close values of Lande g-factors of $|g, F = 4\rangle$ ($g_g = 1.00$) and $|b, F = 5\rangle$

($g_b = 1.01$) levels. Still, the strength of the transitions differ significantly as it is shown in Fig. 5.a (red empty circles) and the atom-field interaction for low m_F states is weaker compared to the 2-level-atom model. Correspondingly, the time needed for an atom in the particular m_F state to be optically pumped to the $m_F = +4$ state (with 90% probability) increases for lower m_F states as shown in Fig. 5.a (blue circles). As a result, our simulations are correct only for high m_F states. For example, for $m_F = +4$ the simulations predict that after applying additional field gradient by the auxiliary coil pair, the initial velocity of atoms which can be efficiently decelerated rises by up to 20 m/s. With the increase of the initial velocity, less atoms from low magnetic sublevels experience sufficient deceleration before they are pumped to the $m_F = +4$ state which reduces the net process efficiency and causes significant deviation of the experimental results from the model.

2. The maximum number of trapped atoms for the 7-beam MOT configuration. According to the simulations, the gain in the number of atoms after adding the “Zeeman” beam should be much larger than observed in the experiment. Besides the factor described in the previous paragraph, the discrepancy can also be caused by improper model of the velocity distribution of atoms compared to the actual atomic beam.
3. The results for the 6-beam MOT (Fig. 2.a and Fig. 5.b). Here, we observe the mismatch of both the optimal magnetic field gradient and MOT beams frequency detuning. Besides the issue with the Zeeman levels structure, we attribute this disagreement to a nontrivial orientation of the quantization axis in the MOT, and hence the spatial variation of the σ^+ polarization component intensity.

The processes described in S3 and S4 lead to losses of atoms from the cooling cycle since the laser radiation is only resonant with the $|g, F = 4\rangle \rightarrow |b, F = 5\rangle$ transition. However, the probabilities of these processes are small [38], so they do not impact the results significantly. In the experiment, we observe a 1.5 times increase of the atoms in MOT when adding a weak (0.2 mW) $|g, F = 4, m_F = 3\rangle \rightarrow |b, F = 5, m_F = 4\rangle$ repump radiation. It repumps atomic population from the $|g, F = 3\rangle$ state. Our observations agree with the effect of the repumping beam from Ref. [38].

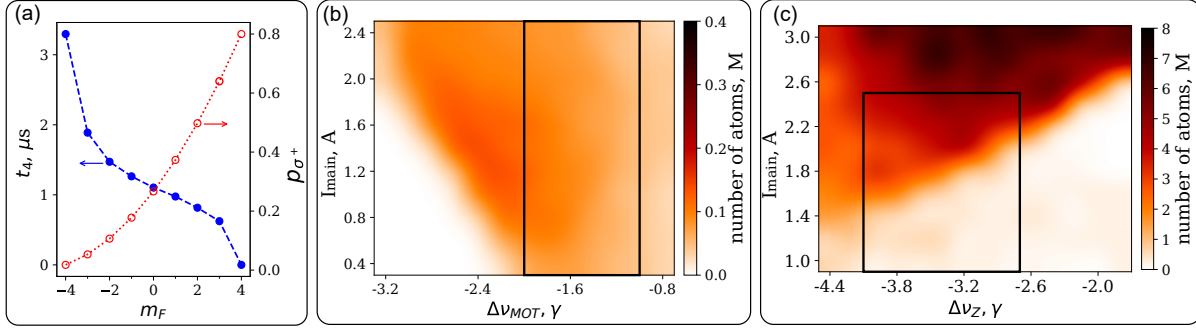


Figure 5: Results of the simulations. (a) Red empty circles: the probability p_{σ^+} of σ^+ transitions relative to the 2-level atom case for different ground state magnetic sublevels m_F . Blue filled circles: time t_4 necessary for an atom to be optically pumped to $m_F = +4$ state for our experimental conditions. (b) Prediction of the number of atoms trapped in the 6-beam MOT as a function of the frequency detuning $\Delta\nu_{\text{MOT}}$ and current through the MOT coils I_{main} . Black box shows the region corresponding to experimentally covered range (Fig. 2.a). (c) Similar results for the 7-beam MOT. The frequency detuning $\Delta\nu_Z$ corresponds to the "Zeeman" beam. Color bars represent the number of trapped atoms in millions.